Performances of a producer gas from sewage sludge gasification enriched with ammonia in a spark-ignition engine

Pierre Brequigny, E. Pacaud, C. Mounaïm-Rousselle

Performances of a Producer Gas from Sewage Sludge Gasification enriched with Ammonia in a Spark-Ignition Engine

P. Brequigny*, E.Pacaud, C. Mounaïm-Rousselle

Université d'Orléans, INSA-CVL, PRISME, EA 4229, F45072 Orléans, France

*corresponding author: pierre.brequigny@univ-orleans.fr

Abstract

Syngas (Synthetic Gas), producer gas or wood gas, are gaseous fuels that could be produced by the gasification of biomass. It is mainly composed of hydrogen and carbon monoxide with a smaller share of methane, all diluted by nitrogen and carbon dioxide. Although it contains carbon in its composition, it is considered as a low or zero carbon fuel as soon as it is made from biomass, which makes it a strong candidate for reducing the global warming impact of combustion engines. This work focuses on the combustion development and performances of a Spark-Ignition engine, fuelled with a synthetic producer gas enriched with ammonia, from a nitrogen-rich sample, typical of ammonia-enriched sewage sludge. Results show that, by replacing part of the producer gas by ammonia, the indicated work increases and the combustion development is slowed down. Last exhaust emissions measurement shows a decrease in CO and CO_2 as a function of ammonia addition in the fuel thus showing that ammonia does not influence the combustion efficiency for the carbon species. Yet a noticeable increase of NOx is observed when adding ammonia to the fuel.

Keywords: sewage sludge, ammonia, syngas, producer gas, combustion, engine

Nomenclature

ATDC After Top Dead Center	P Pressure
BTDC Before Top Dead Center	Q Heat
BBDC Before Bottom Dead Center	RPM Revolutions Per Minute
CAD Crank Angle Degree	SIT Spark Ignition Timing
CAXX CAD where XX % of the fuel is burned	S_L^0 Laminar flame speed
COV_{IMEP} Coefficient of IMEP variation	T Temperature
HC Total Hydrocarbons	$\dot{V}$ Volumetric Flowrate
HRR Heat Release Rate	V_{cyl} Diplaced Volume
IMEP Indicated Mean Effective Pressure	W Work
LHV Lower Heating Value	α Crank angle
m_{fuel} Fuel mass	γ Heat capacity ratio

1 Introduction

The Intergovernmental Panel on Climate Change IPCC (https://www.ipcc.ch/) report has brought clear insight concerning climate change with the estimated global warming scenarii. The most optimistic forecast expects a 2°C global warming for the next century. To limit it as much as possible, the global emissions of the Greenhouse Gases (GHG) must significantly decrease in the next few years. Electricity and Heat production along with Agriculture Forestry and other Land Use (AFOLU) contribute to half of these world's emissions.

The agro-industrial feedstock such as the municipal sewage sludge is a source of renewable gases making them attractive fuels. These gaseous fuels can be obtained by different process as hydrothermal gasification (375-500°C), gasification (800–1000°C) and methanization/anaerobic digestion (40°C). The choice between wet and dry processes

depends on the nature of the feed and its water content. Among these processes, anaerobic digestion can take place in the presence of water and is suited for the valorization of wet feedstock, such as wet animal manures and municipal sewage sludge (SS). Yet, anaerobic digestion (producing mainly methane and CO_2) requires a long retention time (about 20 days) and generates a significant amount of residues (digestate), which is sensitive to pollutants especially when processing sewage sludge. On the other hand, gasification or pyro-gasification is also well suited for biomass with low water content, such as agricultural and forestry waste but wet wastes can also be used if a drying step is applied on them. As demonstrated by Wu et al. [1], GHG emissions from agriculture can be reduced by changing the current use of manure by using gasification. This process shows an improvement regarding waste's life cycle and a GHG emissions reduction turning biomass into energy supply. By using such fuel in a cogeneration process or an electricity power unit, it would enable locally better waste management while providing sustainable energy and could potentially reduce GHG emissions from both the energy and agricultural sectors.

The purpose of a gasification system is to transform solid fuels (crude biomass or char obtained from pyrolysis or hydrothermal carbonization) into combustible gaseous mixtures. The gaseous products, mainly composed of hydrogen (H_2), carbon monoxide (CO), methane (CH_4), nitrogen (N_2) and carbon dioxide (CO_2) forming syngas, can be used after a cleaning process as a gaseous fuel for thermal energy converter. One gasification challenge is to keep the gas free of corroding or regulated components (i.e. H_2S, NH_3, …) prior to subsequent combustion and power generation. As a waste-to-energy process, biomass thermal conversion competes with landfilling and methanization, but the carbon utilization of the syngas road is higher than landfilling [2] and can be in some case better than the biogas road (anaerobic digestion) [3]. Methanization is limited where livestock manure can be considered as waste when it is in surplus, especially in areas with structural nitrogen surplus. Indeed, the nitrogen

concentrated in the digestate limits its spreading in this situation because of possible ammonia emission and soil and water contamination.

Yet, the thermal conversion remains challenging because the properties of the producer gases, thus its combustion potential, vary significantly with the feedstock characteristics (chemical composition, moisture content, structure, reactivity, physical properties, impurities, etc.) [4–7], the gasification reactor type [8] and the key operating parameters (temperatures, reaction atmosphere, stoichiometric ratios, gas flow rates and heating rates) [9–11]. During the gasification, different impurities (nitrogen-impurities, sulphur-impurities, and chloride-impurities) may be produced favourably [12,13], depending on their quantity in the original sample [14]. Agro-industrial manures and SS have similar properties with higher nitrogen (N) and water contents produced in large quantities, and therefore are considered good candidates for energy production. Thus, many efforts have been made to investigate the N conversion during sewage sludge pyrolysis [15,16]. During the thermal conversion, nitrogen is released as nitrogen-containing volatiles including NOx precursor gases such as ammonia (NH_3) and hydrogen cyanide (HCN). Besides, the composition of these volatiles is dependent on the process applied and temperature range. The nitrogen conversion and the emission of nitrogenous compounds (NH_3, HCN) or N-Tar yields production is strongly dependent on the temperature [15], the heating rate, and the residence time [16]. Hence, such feedstocks provide favourable conditions for the yield of N-impurities such as ammonia. The amount of ammonia in the producer gas depends mainly on the nitrogen content of feedstock. Yet, not all the nitrogen is converted into ammonia during the process. Schweitzer et al. [4] showed a linear relationship between the ammonia content in the gas and the nitrogen content of the feedstock. With three different feedstocks, namely cattle, pig manure and sewage sludge, they obtained 1.9 , 2.2 and 6.6% Vol. of ammonia in the sygas respectively. With sewage sludge and a blend of 40%/60% mass sewage-sludge and coal, Pinto et al. [11] were able to obtain

2.2 and 2% of ammonia in the syngas respectively. However, in most processes, especially engines for Combined Heat and Power (CHP), these undesired yields are avoided as much as possible to obtain a "purer" syngas, i.e. mostly composed of H_2 and CO.

The use of syngas or producer gas in thermal energy converters dates back to World War II when gasoline shortages stimulated the conversion of vehicles to fuel derived from wood gasification. A renewed interest appeared in the last decade with a use of syngas/producer gas in CHP application. Despite being a well-established technology, researches on the characteristics of syngas fuelled energy converters are limited especially considering the composition impact. As underlined in the review of Fiore et al. [17]: "difficulties in predicting the actual flame speed essentially derives from the wide variability of syngas composition, which results from a number of factors related to its production technology" or the nature of the feedstock as underlined above. The questions are therefore what could be the impact of the syngas/producer gas composition on the combustion as a function of the feedstock type and how the presence of impurities in the gas would affect the engine performances (possibly in a CHP system). If the presence of these impurities does not affect the gasification process itself, nor the thermal conversion via combustion, the overall cost of resource recovery would decrease due to one less step. It is, nonetheless, necessary to have a flexible and robust installation to provide the highest efficiencies whatever the producer gas or syngas compositions.

As for application, syngas/producer gas is nowadays successfully used in thermal converters based on spark-ignition (SI) engines. However, since those kinds of engines are usually designed and optimized for gasoline or natural gas, specific arrangements are required to operate on syngas. The important variability of composition exacerbates this issue decreasing operation stability when the producer gas quality is low and strengthen the need of optimizing operating parameters through prevention and regulation systems. Moreover, the use of

producer gas generally results in a decrease in engine power, which can be compensated by either increasing the compression ratio as much as possible (but limited by knock occurrence), as highlighted by Sridhar et al. [18] and by Szwaja et al. [19,20] for a producer gas, or by turbocharging. As underlined by Fiore et al. [17], a significant number of studies, both numerical and experimental deals with the use of syngas in SI engines. However, most of them focus on the knock limit strongly affected by the syngas' composition. Studies on the impact of the composition in SI engine by considering a complete producer gas composition (not only H_2/CO blends) are quite sparse. Arunachalam and Olsen [21] studied the knock propensity as a function of different compositions. Their work is noticeable since it compares "real" compositions containing all the main components of the producer gas namely H_2, CO, CH_4, CO_2 and N_2. Bhaduri et al. [22] fueled a compression ignition engine in homogeneous combustion mode by connecting directly a gasifier, which results in composition variation as a function of the gasification process evolution over time. Recently, Rabello de Castro et al. [23] studied 3 different compositions previously identified by Bridgwater [8], in a dual-fuel compression ignition engine. They showed that: i) H_2 content has a strong influence on the Heat Release Rate as well as on the combustion phasing and duration; ii) the presence of CO_2 in the producer gas plays an important role in reducing NOx emissions but too much CO_2 can lead to poor efficiency and emissions increase; iii) the combustion development can be empirically predicted by fundamental properties of the syngas/producer gas composition such as laminar flame speed or adiabatic flame temperature. One other interesting study was proposed by Tsiakmakis et al. [24] with the use of three different compositions in SI engine coming from three different feedstocks namely olives, peaches and grapes and showed interesting engine performances but pollutant emissions were not measured. They blended these compositions with propane and compared it with pure propane showing that increasing the syngas content leads to reduced in-cylinder pressures, heat release rates and power output

but that stable operation is ensured with a power output reduction less than 10% for mixtures of 55% w/w producer gas and 45% w/w propane compared to neat propane. Thus, the impact of impurities on engine operation is not well covered by the literature currently and considering that N impurities can lead to NOx emissions at the exhaust, this requires quantification.

Moreover, ammonia recently gains a renew interest has a potential zero-carbon fuel in internal combustion engine especially in Spark-ignition (SI) ones. Indeed, despite his unfavorable combustion properties [25], stable operation were achieved with neat ammonia in SI engines with different architectures [26–31]. It could be also noticed that one of the first use of ammonia in engines dates back to WWII in Belgium, where the bus fleet operated with the first dual fuel engine ever reported: coal gas (so similar to syngas) composed of 50% H_2 directly injected in the combustion chamber filled with ammonia [32].

The objective of this study is therefore to consider this ammonia content no longer as an impurity but as part of the fuel. For this purpose, a producer gas composition representative of sewage sludge gasification (likely to contain ammonia) is selected and investigated in a Spark-Ignition engine in terms of performances and emissions. For reference, the synthetic producer gas (reproduced from gas bottles) is first compared to pure methane. The second part of the present paper studied the effect of blending ammonia with producer gas on the engine performances and emissions to assess its impact either considered as an impurity or a co-fuel by varying the ammonia share in the blend.

2 Experimental Setup

2.1 Engine characteristics

The experiments were conducted in a research single cylinder SI engine. All specifications are presented on the Table 1.

Table 1: Engine specifications

Displaced volume	535.5 cm^3
Bore	77 mm
Stroke	115 mm
Connecting rod length	177 mm
Compression ratio	11.7
Intake valve opening	5 CAD After Top Dead Center (ATDC)
Exhaust valve opening	5 CAD Before Bottom Dead Center (BBDC)

For all operating conditions, the engine is driven by an electric motor at a fixed engine speed of 1400 rpm. The engine speed for genset application is usually 1500 RPM. Unfortunately, it was not possible with the present setup due to important vibrations of the intake/exhaust pipes and bench. The optical encoder placed in the main crankshaft enables the monitoring of the angular position with a 0.1 Crank Angle Degree (CAD) resolution. The bench is described in more details by Mounaïm-Rousselle et al. [31]. The in-cylinder pressure is measured using a Kistler piezoelectric pressure transducer (6045A) (accuracy of $\pm$ 2%). Intake and exhaust temperature and pressure are monitored using K-type thermocouples and piezoresistive absolute pressure transducers respectively. The absolute in-cylinder pressure is obtained by its equalization with the average absolute pressure at the inlet, Pin, at 20 CAD after the intake valve opening. The charge duration for the ignition coil was set to 2 ms. For all the data presented below, the Spark Ignition Timing (SIT) was optimized to obtain the maximum

Indicated Mean Effective Pressure (IMEP), with a covariance, COV_{IMEP} , below 5%.

All gaseous flows except air, are measured and controlled using Brooks thermal mass flowmeters precision to ensure control of the equivalence ratio. The uncertainty for NH_3, N_2, CO flow is about $\pm$ 0.9% of the full scale (100 NL/min) and for H_2, CO_2, CH_4 it is about $\pm$ 1% of the full scale which is respectively 50, 37 and 5 NL/min. For air, an EMERSON F025S was used with an uncertainty of $\pm$0.5% of the full scale (1100 NL/min). The resulting uncertainty on the equivalence ratio is $\pm$2%. All gases are preheated to the intake temperature of 30°C and premixed in a plenum before their introduction into the combustion chamber. The engine exhaust emissions were measured with the Horiba MEXA 7100HEGR. This exhaust gas analyser measures CO and CO_2 (non-dispersive infrared absorption analyser), NOx (chemiluminescence analyser), O_2 (magneto-pneumatic detector) and unburned hydrocarbon (HC) (flame ion analyzer) with a precision of 1 ppm for all gases. As these results are given in dry share (except for HC), a calculation considering the share of water vapour in the exhaust enables to readjust the content of each gas. A global scheme of the experimental setup is displayed in Fig. 1.

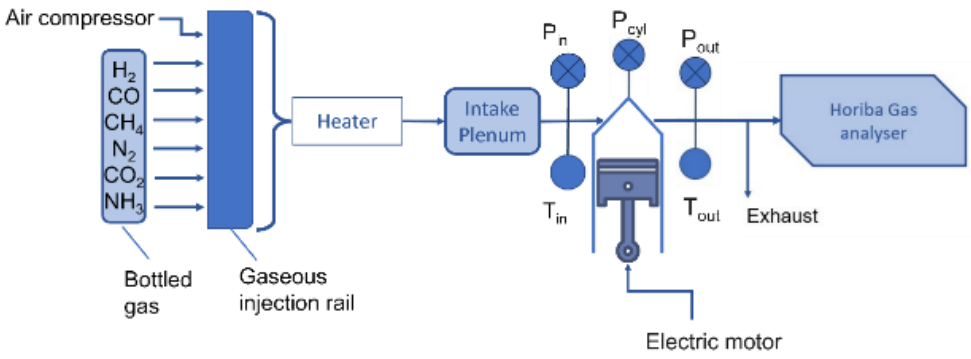

Figure 1: Layout of the experimental setup

For each condition, the test was repeated three times, to check repeatability. A standard deviation less than 1% was obtained on the main parameters (IMEP, maximum pressure,

combustion duration, COV_{IMEP}). For each test, 100 cycles were acquired. Results in terms of pressure, heat release rate, IMEP, efficiencies, combustion duration are computed from the averaged pressure signal over 100 cycles.

2.2 Producer gas composition

A producer gas composition from the gasification of sewage sludge was chosen to evaluate its combustion characteristics. This kind of feedstock is usually nitrogen-rich and able to produce ammonia as impurity when gasified. The composition chosen for this study was the one from Szwaja et al. [19] which was configured to be in an optimal gas production condition. This composition is displayed on Table 2 and will be blended with ammonia to evaluate the impact of ammonia in combustion development in a spark-ignition engine. This selected composition was used in a similar engine by Szwaja et al.. Yet, since the composition is reproduced from gas bottles in the present study, tar content is not considered. It could be added that the composition is also quite similar to the Updraft composition obtained by Bridgwater [8] (based on wood pellet) : same amount of CH4 and N2, similar H2 content, but less CO and more CO2. Therefore, the present composition leads to a lower LHV. It can be noted that this reference composition from Bridgwater was recently used in different fundamental combustion [33,34] and engine[23] studies.

Table 2: Producer gas composition from Szwaja et al. [19]

Gas	H_2 %mol	CO %mol	CH_4 %mol	CO_2 %mol	N_2 %mol
Content	13.00	16.00	3.00	15.00	53.00

The stoichiometric ammonia-added producer gas reaction can be expressed as follows:

$$aH_2 + bCO + cCH_4 + dCO_2 + eN_2 + \left(\frac{a}{2} + \frac{b}{2} + 2c + \frac{3}{4}x\right)(O_2 + 3.76N_2) + xNH_3 \rightarrow (a +$$

$$2c + \frac{3}{2}x)H_2O + (b + c + d)CO_2 + (e + 3.76\left(\frac{a}{2} + \frac{b}{2} + 2c + \frac{3}{4}x\right) + \frac{x}{2})N_2 \qquad (1)$$

From Eq. 1, air-fuel ratios and mole fraction of each gas based on the equivalence ratio are calculated for all conditions.

2.3 Experimental conditions

For this study, methane was firstly used as a reference fuel with three equivalence ratios as displayed in Table 3. These values provide a relevant comparison with producer gas in the same conditions, and then with ammonia-added producer gas, for two different intake pressures. The amount of ammonia in the fuel blend was incremented by 2.5% up to 10%Vol. then with a last point at 15%, to observe the impact of ammonia 'impurity' on the producer gas performance. Table 3 summarizes all experimental conditions of this study and Table 4 displays the main characteristics for each blend.

Table 3: Engine test condition, N=1400 rpm, intake temperature T_{in}=30°C

Fuel	Equivalence Ratio (ϕ)	%Vol. NH_3 in the fuel	Intake pressure P_{in} (bar)
CH4	0.9;1;1.1	0	1
Producer gas	0.9;1;1.1	0	1;1.2
Producer gas + NH_3	1	0;2.5;5; 7.5;10;15	1;1.2

Table 4: Mixture properties

Fuel composition	Stoichiometric air-fuel ratio (AFR^{st})	LHV of the fuel mixture ($MJ.kg^{-1}$)	Energy per kg of air ($MJ.kg^{-1}$)
Methane	9.52	50.33	5.29
100% producer gas	1.51	3.35	2.22
97.5% producer gas 2.5% NH_3	1.47	3.53	2.39
95% producer gas 5% NH_3	1.44	3.71	2.58
92.5% producer gas 7.5% NH_3	1.40	3.89	2.78
90% producer gas 10% NH_3	1.36	4.08	3.00
85% producer gas 15% NH_3	1.29	4.44	3.46

2.4 Post Processing

The Apparent Heat Release Rate (HRR) is calculated from the in-cylinder pressure as follows:

$$\frac{dQ}{d\alpha} = \frac{\gamma}{\gamma - 1}.P.\frac{dV}{d\alpha} + \frac{\gamma}{\gamma - 1}.V.\frac{dP}{d\alpha} \quad (1)$$

Where γ is the heat capacity ratio, P the in-cylinder pressure, V the in-cylinder volume and α the CAD. Only the net heat release rate is calculated, heat losses were not estimated. The HRR is initially computed with a constant heat capacity ratio to estimate the share of burnt

and unburnt gases as a function of the crank angle. From this first estimate of burnt and fresh gases share, the composition inside the combustion chamber is computed at each CAD. Knowing the composition and the temperature (from the perfect gases assumption), the heat capacity ratio is calculated (from the BURCAT polynomial coefficient [35]) as function of the composition and the temperature at each CAD. Then, the HRR is computed a second time with this variable γ depending on the gas composition and temperature at each CAD.

The indicated efficiency is computed as follows:

$$\eta_i = \frac{W_{ind}}{Q_{fuel}} = \frac{IMEP.V_{cyl}}{m_{fuel}.LHV_{fuel}} \tag{2}$$

where W_{ind} corresponds to the indicated work, Q_{fuel} the energy content of the mixture, $IMEP$ the indicated mean effective pressure, V_{cyl} the displaced volume, m_{fuel} the mass of the fuel and LHV_{fuel} the lower heating value of the fuel.

Two methods have been established regarding the combustion efficiency. The first one computes the efficiency by taking into consideration the unburnt or partially burned exhaust gases with this equation as follows:

$$\eta_c^{pollu} = 1 - \frac{\dot{V}_{HC}LHV_{HC} + \dot{V}_{CO}LHV_{CO}}{\dot{V}_{fuel}LHV_{fuel}} \tag{3}$$

Where $\dot{V}_{HC}$, $\dot{V}_{CO}$ and $\dot{V}_{fuel}$ are respectively the normal volume flow rate of hydrocarbon, carbon monoxide and fuel multiplied by their Lower Heating Value in MJ/L. It is considered that the Lower Heating Value of HC is equal to the one of the CH_4.This method must include all unburned or partially burned gases to be totally accurate. Since not all these gases can be assessed from the analyser, this method is only an estimate of the combustion efficiency considering only the hydrocarbon and carbon monoxide reactions.

The second method is based on oxygen balance between intake and exhaust and computed as follows:

$$\eta_c^{O_2} = 1 - \frac{O_{2_{exhaust}}}{O_{2_{intake}}} \quad (4)$$

Where $O_{2_{exhaust}}$ and $O_{2_{intake}}$ are the normal volumetric flow rate of oxygen at the exhaust and at the intake respectively.

2.4 Kinetics simulation setup

Numerical simulations were carried out using the premixed laminar flame-speed calculation module PREMIX of ANSYS CHEMKIN-PRO [36] to estimate the laminar flame speed and adiabatic flame temperature in engine conditions. Simulations were carried out with an average number of 1000 meshes on a 10 cm grid, a curvature of 0.1, and a gradient of 0.05 with 5 continuations. The selected mechanism is the one of Okafor et al. [37] since it is one of the only ones able to simulate producer gas/ammonia blend. This mechanism is based on the GRI-Mech 3.0 [38] for the carbon chemistry, well suited for methane and natural gas and on the mechanism of Tian et al. [39] for ammonia chemistry. It consists in 59 species and 356 elementary reactions and was validated on laminar flame speed of methane/ammonia mixture with an ammonia energy share up to 30% of the total energy content, at atmospheric conditions, i.e 1 atm and 298 K, and equivalence ratios ranging from 0.8 to 1.3. In our case, the 90%Vol. producer gas/10 %Vol. ammonia blend corresponds to an ammonia energy share of 33% and the 15%Vol. ammonia blend corresponds to 53% of ammonia energy share.

3 Results and Discussion

3.1 Producer gas versus methane

Figure 2 displays the in-cylinder pressure of methane and producer gas for three equivalence ratios. As expected, the maximum of pressure obtained with producer gas as fuel is lower than for methane only, not really affected by the equivalence ratio, where the maximum of pressure is around 42 bar.

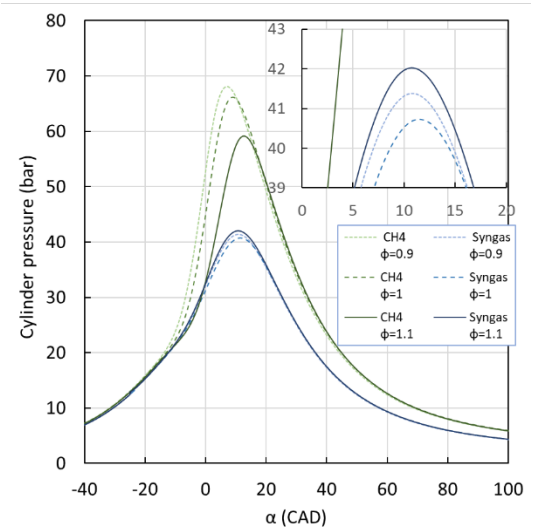

Figure 2: In-cylinder pressure evolution for producer gas compared to pure methane for three equivalence ratios at 1 bar intake pressure.

As consequence, the IMEP for pure producer gas is lower than for methane only, respectively 5.5 bar and 9 bar as it can be seen in Fig. 3, due to the presence of high amounts of inert gases (N_2=53% and CO_2=15%) which induces lower LHV and lower energy input. These results are in good agreement with those from Szwaja and Cupial [20]. The increase of the intake pressure (from 1 to 1.2 bar) enables a higher IMEP thus showing potential for boosted operation especially without any knock occurrence recorded with this composition. This way, even though methane combustion is more efficient than producer gas, the increase of intake pressure could be a way to compensate the performance depletion provoked by producer gas. For both fuels, the combustion was stable with COV_{IMEP} between 0.74% and 1.5% for methane and 0.9% on average for producer gas.

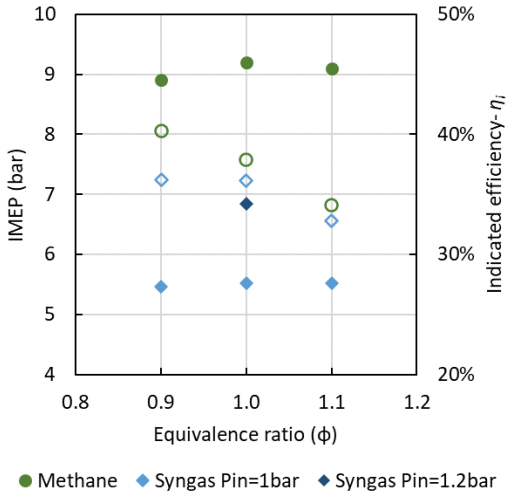

Figure 3: IMEP (filled symbols) and Indicated efficiency (empty symbols) of producer gas compared to methane as a function of the equivalence ratio

From Figure 3, it can be noted the decreasing trend of the indicated efficiency can be observed with both gaseous fuels as the air/fuel ratio increases, with also lower values reached for producer gas fuel than methane only (36% and 38% at ER=1 and 36% and 40% at ER=0.9, respectively). The heat release rate comparison between producer gas and pure methane as a function of ϕ is shown in Figure 4. Its evolution tends to follow the in-cylinder pressure one due to LHV and energy input difference (about 0.82 kJ for producer gas vs. 1.20 kJ for CH_4): a maximum peak at 27 J/CAD for producer gas at ER=1.1 against 76 J/CAD for methane at ϕ=1. However, the HRR evolution is wider for producer gas than methane, which means that the combustion duration is longer.

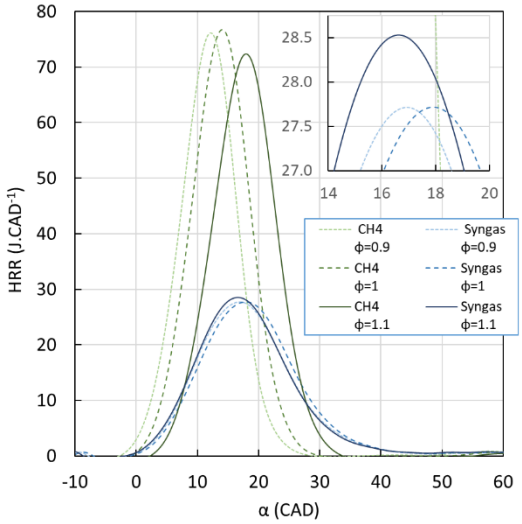

Figure 4: Net heat release rate of producer gas and methane for several equivalence ratios at 1 bar intake pressure

This difference is highlighted in Figure 5 where the three different combustion phases are given : from the start, i.e. early flame kernel development (CA10-SIT), the mid, i.e. self-sustained propagation (CA50-CA10) to the end, i.e. post-flame combustion (CA90-CA50), with the variable CAXX, representing the crank angle degree when XX% of mass is burned. As shown in this bar chart, the producer gas has a longer combustion mainly during the first phase (20 CAD for producer gas against 15 CAD for methane only). As highlighted in [33,34], the laminar flame speed of a similar producer gas composition is much smaller than for methane. As the laminar flame speed is one of the main parameters driving the combustion process in Spark-Ignition engine, it is one of the main reasons for the slower combustion explained by the dilution effect of nitrogen and carbon dioxide within the producer gas (68% vol. of CO_2+N_2). This figure also shows the negligible impact of the equivalence ratio on the different combustion phases for the producer gas in contrary with the methane whose combustion duration decreases when increasing the equivalence ratio up to 1.1 corresponding to the maximum laminar flame speed.

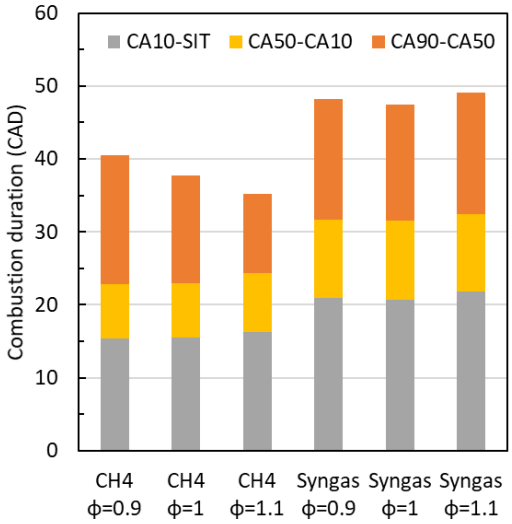

Figure 5: Combustion duration analysis comparing methane and producer gas as a function of the equivalence ratio at 1 bar of intake pressure

The emission comparison between methane and pure producer gas is displayed in the Figure 6. As expected, the CO_2 emissions for producer gas (17%) is twice that of methane (8%), due to the presence of CO_2 in producer gas composition (15%). NOx and unburnt HC are lower for producer gas, respectively 50ppmv and 720ppmv, than for methane (1500ppmv and 2130ppmv), at ϕ=1. The amount of NOx produced with methane as fuel is due to the highest temperature, favouring thermal NOx formation. The specific composition of the producer gas tends to provoke similar effect than the dilution by exhaust gas recirculation (EGR), preventing thermal NOx production due to the decrease of the combustion temperature. By considering HC and CO emissions, the difference induced by the two fuels might be related to the lower carbon content of the producer gas. As a function of the equivalence ratio, no real impact can be noted for the producer gas; contrary to the case of methane, as already well studied in literature [40]. NOx emissions increase in lean side (4300 ppmv at ER=0.9 versus 320 ppmv at ER=1.1) as expected but HC and CO emissions respectively follow the opposite trend. It is surprising to note that HC and CO for the producer gas are very low without any increase on the rich side. Similar results were found recently in the literature by Bui et al [41]

and Sharma et al. [42] who measured very low HC and CO concentrations with a similar producer gas in similar engine operating conditions. Shah et al. [43] also observed a decrease up to 96% for CO when switching from gasoline to producer gas and attributed it to the lower carbon content of producer gas. In the present case since the producer gas is highly diluted (68%Vol. of N2+CO2) the CO share in the total mixture is very low. For HC, since the only source in the producer gas is the small amount of CH_4, HC emissions could be attributed to the lubricant oil and are not affected by the air/producer gas equivalence ratio.

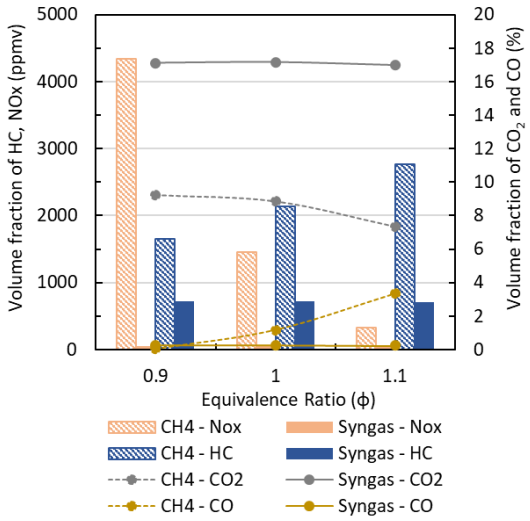

Figure 6: Comparison of exhaust emissions for producer gas and pure methane for 3 equivalence ratios at 1 bar of intake pressure

3.2 Producer gas blended with ammonia performances

Figure 7.a. and b. show the in-cylinder pressure and HRR evolution as a function of ammonia addition in producer gas at 1.2 bar intake pressure and ϕ=1.0. Their peaks values do not seem affected by the presence of ammonia in the fuel, only a small change on combustion duration can be distinguished. Since IMEP is the integral of the in-cylinder pressure, more indicated work is then obtained when ammonia is added due to the increase of LHV and energy input (Table IV) , as it can be seen in Figure 8, for 1 bar and 1.2 bar intake pressure.

According to this figure, the addition of NH_3 to the producer gas' mixture increases the IMEP. As expected, and already highlighted for pure producer gas, the 20% intake pressure increase enables to increase the IMEP of more than 1 bar, more than 22%, without any knock occurrence as expected especially since the intake temperature is the same for both intake pressures.

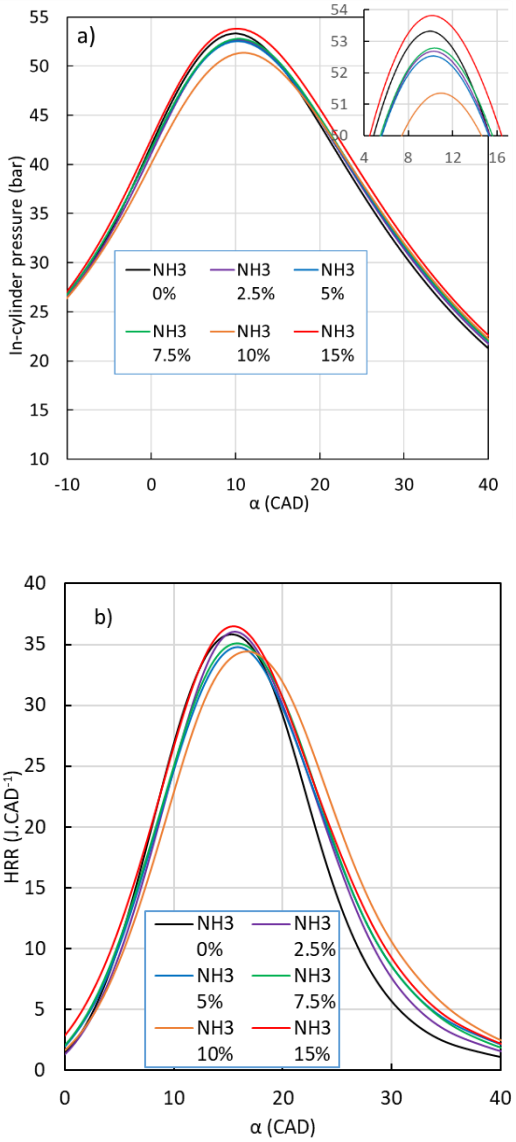

Figure 7: In-cylinder pressure (a) and HRR evolution as a function of ammonia content (%Vol). in the producer gas/ammonia blend at 1.2 bar intake pressure – ϕ=1

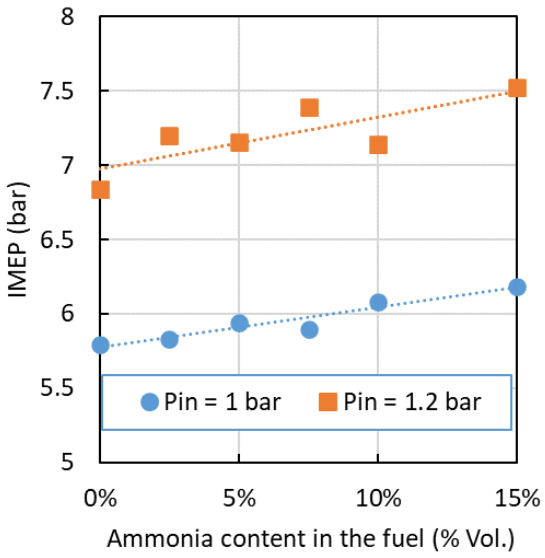

Figure 8: IMEP of engine running on producer gas as a function of the ammonia content for both intake pressures – ϕ=1

Figure 9 displays the evolution of optimized spark ignition timing (SIT) as a function of ammonia content in the producer gas/ammonia blend. The optimized value is set when the IMEP is at its highest. When ammonia is added, the SIT must be advanced (from 23 CAD with pure producer gas to 35 CAD with 15% ammonia). These SIT guarantee stable conditions whatever the ammonia content in the blend with a COV_{IMEP} around 1%, apart 15% ammonia at 1.2 bar, where COV_{IMEP} reaches up to 4%.

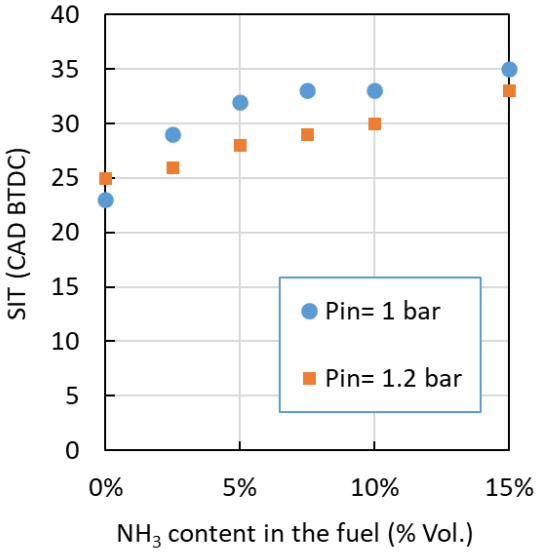

Figure 9: Optimised SIT as a function of ammonia content in producer gas for two intake pressures – ϕ=1

Figure 10 shows the evolution of indicated efficiency as a function of the ammonia content in producer gas: for both intake pressures, a slight decrease can be observed with the increase of ammonia content from η_i=36% for pure producer gas until 35% when 15% ammonia is added. This decrease remains yet restrained without significant tendency with the intake pressure increases.

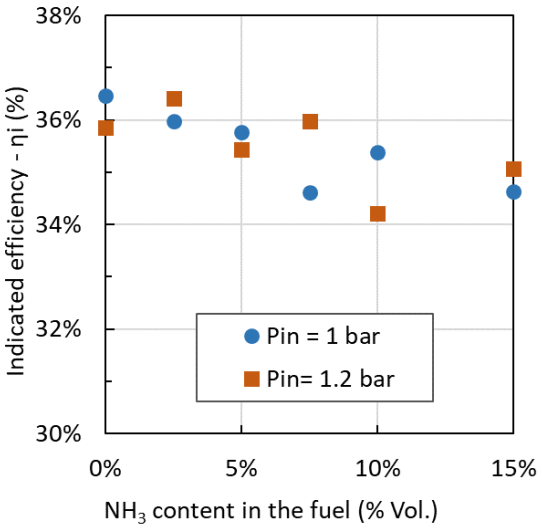

Figure 10: Indicated efficiency as a function of ammonia content in the blend for both

intake pressures – ϕ=1

The slight decrease of the indicated efficiency can be partly explained by the increase of the combustion durations especially during the first half of the combustion as highlighted in Figure 11. It can be seen that the greater the ammonia concentration is, the longer the start of the combustion will last, mainly due to the low flame speed of ammonia as demonstrated in Lhuillier et al. [25,29]. Since the spark-timing is kept at optimum phasing, i.e. maximizing IMEP, a longer combustion duration will result in a lower indicated work relatively to the energy introduced in the cycle.

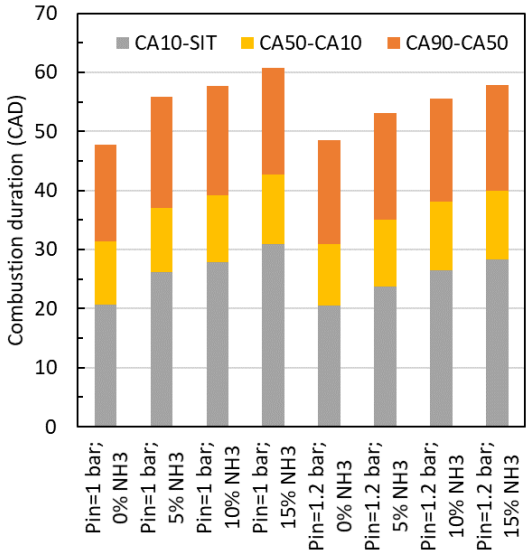

Figure 11: Combustion duration analysis of producer gas as a function of the ammonia content in the blend for both intake pressures – ϕ=1

To confirm this analysis, CA10-SIT and CA50-CA10 are plotted against the laminar flame speed estimated by kinetics OD simulations with the in-cylinder pressure and temperature at SIT conditions as initial conditions. Figure 12 indicates how the initiation phase strongly depends on the laminar flame speed: the higher the flame speed the shorter the CA10-SIT. The highest flame speed (65.1 cm/s) is reached for pure producer gas and the lowest (29.1 cm/s) for the 15% NH_3 in blend. Yet, the decrease of the flame speed as function of the

ammonia content in the blend is twofold: i) the lower flame speed of ammonia which decreases the flame speed of the blend; ii) because of this lower flame speed, the SIT value must be advanced to keep the best IMEP with the lowest cycle to cycle variations (Figure 9), thus leading to different in-cylinder pressure and temperature conditions. During the initial phase, the flame is not yet strongly affected by the turbulence inside the combustion chamber. On the contrary, for the self-sustained propagation phase, i.e. CA50-CA10, the combustion duration is constant as function of the laminar flame speed. Once the combustion is well initiated, i.e. after CA10, the flame-turbulence interaction would enable a better oxidation of the fuel, counterbalancing the impact of ammonia.

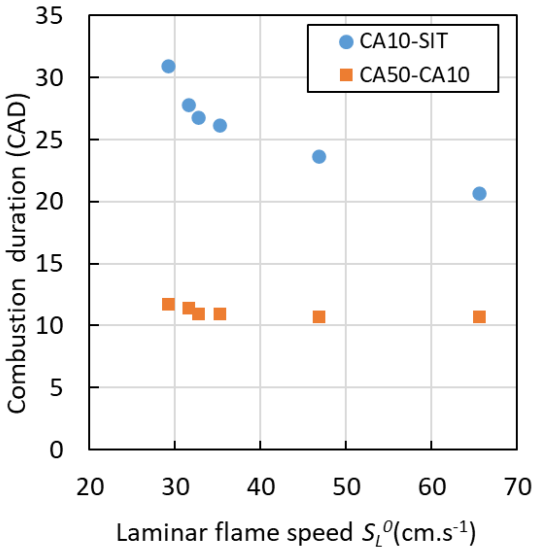

Figure 12: Combustion duration as function of the laminar flame speed calculated at SIT conditions and for intake pressure of 1 bar – ϕ=1

The Figure 13 displays the evolution of the exhaust emissions as function of the ammonia content. Once ammonia is introduced into the fuel, the NOx emissions increase drastically: from 50 ppmv without ammonia to 2000 ppmv with just only 2.5% of ammonia in the fuel. However, after this jump, NOx emission is not sensitive to the ammonia content and remains around 2100 ppmv, due to the different kinetic mechanisms of nitrogen "fuel road" [44],

involving a set of recombination reactions between ammonia and oxygen to form NOx especially for low concentrations of ammonia. Indeed, the adiabatic flame temperature (estimated with kinetics simulations with Ansys CHEMKIN-Pro as laminar flame speed), one parameter to enhance thermal NOx production, is not really affected by this small addition of ammonia: about 2130 K constant from 0 to 7.5% of ammonia and a slight increase up to 2165 and 2186 K for 10 and 15% NH_3 respectively. The combustion efficiency might explain the stabilisation of NOx emissions as the amount of unburned ammonia tends to rise which prevent from further oxidation and thus NOx production. Besides, when increasing the concentration of ammonia, the unburned ammonia could be responsible for a reduction of NOx inside the combustion chamber, as it is for instance in a SCR system. It is interesting to note that very similar trends were obtain with CH_4/NH_3 blends in a mild combustor by Ariemma et al [45]. The concentration of NOx at the exhaust drastically increases from 5% of Ammonia in the blend and then shows stagnation with a further increase of NH_3 share in the fuel. Ariemma et al. attributed this behaviour to the OH and NH_2 radicals. As they reported, adding even a small quantity of NH_3 could increase the OH production thus boosting the NOx formation through a higher NH_2 selectivity to NO. Moreover, considering the increase of the combustion duration, the in-cylinder temperature might change when adding ammonia thus impacting the NOx formation. Since the HORIBA analyser cannot measure ammonia at the exhaust, those statements are still uncertain, and it is not clear if this stabilisation is caused by a mitigation between the high NOx concentration and oxidation or if the combustion of ammonia is incomplete.

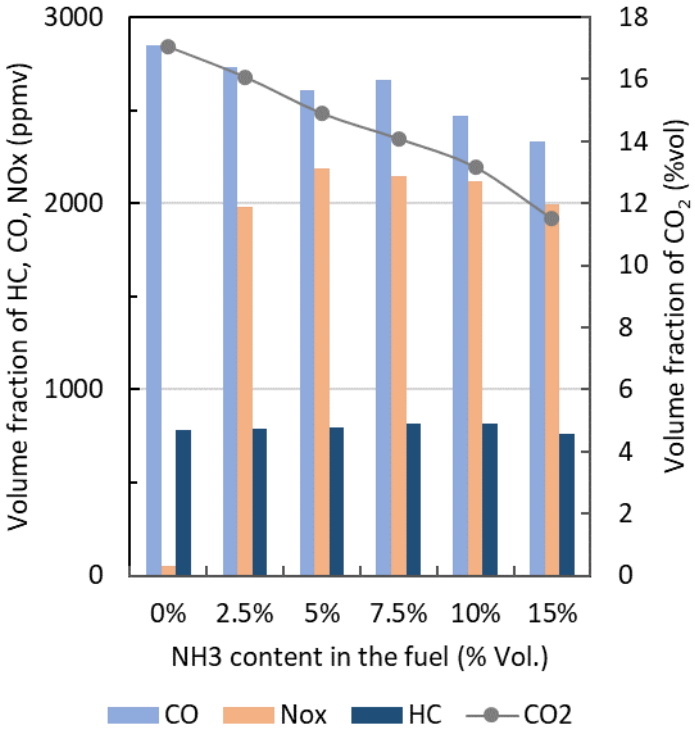

Figure 13: Evolution of producer gas emissions as function of ammonia content at 1 bar intake pressure

The Figure 14 shows the evolution of the combustion efficiency with the addition of ammonia content by using Eq. 4 and 5. As observed, the combustion efficiency calculated from pollutants (Eq. 4) seems stable through the entire campaign with a 98.2% average efficiency at 1 bar intake and a 98.3% average efficiency at 1.2 bar intake. This result proves the low impact of the exhaust gases HC and CO on the combustion efficiency regardless of the intake pressure and ammonia content. The second estimate (Eq. 5) clearly indicates a decreasing trend with the addition of ammonia from 94% with 0% NH_3 to 87% with 15% NH_3 at 1 bar intake pressure, highlighting that a larger part of the fuel is unburned as the ammonia is added. Unlike the first approach, the second one considers the unburned part of ammonia in the exhaust gas. As seen above, since the combustion efficiency is not affected by the HC and CO, its decrease is mainly due to the rise of unburned part of ammonia as the share of ammonia in the producer gas increase. Also, increasing the intake pressure tends to improve

the combustion efficiency from 86.9% with 15% NH_3 at 1 bar to 93.9% with 15% NH_3 at 1.2 bar. Hence, a fewer quantity of unburned ammonia might be present in the exhaust gas at higher intake pressure. The O_2 combustion efficiency decrease as function of the ammonia content is also less pronounced when increasing the intake pressure: from 97% at 0% NH_3 down to 94% at 15% NH_3.

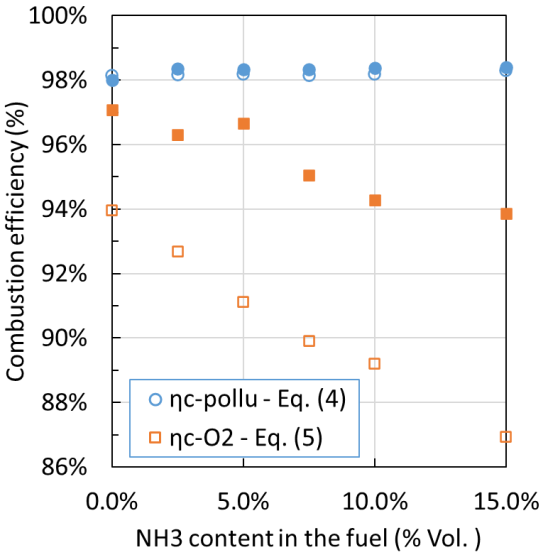

Figure 14: Combustion efficiency of producer gas as a function of ammonia content calculated from Eq.4 and 5. Empty symbols: intake pressure of 1 bar; Filled symbols: intake pressure of 1.2 bar

4 Conclusion

In this work, a producer gas composition, representative of sewage sludge feedstock on SI engine performances and exhaust emissions was studied. First, a comparison with pure methane was established and confirmed that the global performances with producer gas were decreased in comparison to those with CH_4 only. However, increasing the intake pressure (only by 20%) showed that slightly boosted operation allows to reach similar performances. In the other hand, fuelled an engine with producer gas exhibits less pollutant emissions than with methane and especially NOx ones. Secondly, producer gas was blended with small

ammonia amount (maximum 15% volume) to evaluate the impact of this impurity specie, which can be present after the gasification process. The presence of ammonia induces an increase of the energy content in the fuel, which provides higher output produced work. Yet with this producer gas specific composition, the presence of ammonia tends to slow down the global flame speed hence to extend the combustion duration and to slightly decrease the indicated efficiency. The NOx emissions of the 15% ammonia-added producer gas were comparable to the methane whereas HC and CO showed lower values for the ammonia-producer gas blend compared to methane. However, for the highest additions of ammonia (10 and 15% vol), the combustion efficiency decreases probably because of the amount of unburned ammonia in the exhaust especially for atmospheric intake pressure.

Thus, ammonia impurities produced through gasification with a N-rich sample might not be as disadvantageous as expected to be used in genset if a catalytic exhaust aftertreatment system is mounted because of the amount of NOx and possible unburned ammonia emissions. The lack of quantification about the exhaust ammonia is also an issue to conclude entirely on the ammonia-added producer gas properties and should be further investigated. It could be also interesting to study experimentally the fundamental properties of ammonia producer gas blends such as laminar flame speed in order to validate potential kinetic mechanisms.

As a perspective, the usage of ammonia could potentially be beneficial in financial and technological terms since it could save a purification process during the gasification or because blending producer gas from waste on one side and ammonia as an e-fuel on the other side could increase the flexibility of the system and prevent from shortage.

5 Acknowledgements

This work was made possible by the financial support of the CNRS/FITe (FR2039):

“Fédération pour l’Innovation et la Transition énergétique”. The Authors are grateful to B.

Raitiere of Univ. Orléans, PRISME for technical support.

6 References

[1]H. Wu, M.A. Hanna, D.D. Jones, Life cycle assessment of greenhouse gas emissions of feedlot manure management practices: Land application versus gasification, Biomass and Bioenergy. 54 (2013) 260–266. https://doi.org/10.1016/j.biombioe.2013.04.011.

[2]B. Dastjerdi, V. Strezov, M.A. Rajaeifar, R. Kumar, M. Behnia, A systematic review on life cycle assessment of different waste to energy valorization technologies, J. Clean. Prod. 290 (2021) 125747. https://doi.org/10.1016/j.jclepro.2020.125747.

[3]F. Ardolino, U. Arena, Biowaste-to-Biomethane: An LCA study on biogas and syngas roads, Waste Manag. 87 (2019) 441–453. https://doi.org/10.1016/j.wasman.2019.02.030.

[4]D. Schweitzer, A. Gredinger, M. Schmid, G. Waizmann, M. Beirow, R. Spörl, G. Scheffknecht, Steam gasification of wood pellets, sewage sludge and manure: Gasification performance and concentration of impurities, Biomass and Bioenergy. 111 (2018) 308–319. https://doi.org/https://doi.org/10.1016/j.biombioe.2017.02.002.

[5]H. Zhan, X. Zhuang, Y. Song, X. Yin, C. Wu, Insights into the evolution of fuel-N to NOx precursors during pyrolysis of N-rich nonlignocellulosic biomass, Appl. Energy. 219 (2018) 20–33. https://doi.org/10.1016/j.apenergy.2018.03.015.

[6]G.-L. Noemí, A. Zainab, A. María, F. Isabel, Exploring the sustainable production of ammonia by recycling N and H in biological residues: evolution of fuel-N during glutamic acid gasification, J. Clean. Prod. (2020) 124417. https://doi.org/10.1016/j.jclepro.2020.124417.

[7]H. Chen, Y. Wang, G. Xu, K. Yoshikawa, Fuel-N Evolution during the Pyrolysis of Industrial Biomass Wastes with High Nitrogen Content, Energies . 5 (2012) 5418–5438. https://doi.org/10.3390/EN5125418.

[8]A.V. Bridgwater, The technical and economic feasibility of biomass gasification for power generation, Fuel. 74 (1995) 631–653. https://doi.org/10.1016/0016-2361(95)00001-L.

[9]M. Aznar, M.S. Anselmo, J.J. Manyà, M.B. Murillo, Experimental study examining the evolution of nitrogen compounds during the gasification of dried sewage sludge, Energy and Fuels. 23 (2009) 3236–3245. https://doi.org/10.1021/ef801108s.

[10] Y.K. Choi, J.H. Ko, J.S. Kim, A new type three-stage gasification of dried sewage sludge: Effects of equivalence ratio, weight ratio of activated carbon to feed, and feed rate on gas composition and tar, NH3, and H2S removal and results of approximately 5 h gasification, Energy. 118 (2017) 139–146. https://doi.org/10.1016/j.energy.2016.12.032.

[11] F. Pinto, H. Lopes, R.N. André, M. Dias, I. Gulyurtlu, I. Cabrita, Effect of experimental conditions on gas quality and solids produced by sewage sludge cogasification. 1. Sewage sludge mixed with coal, Energy and Fuels. 21 (2007) 2737–2745. https://doi.org/10.1021/ef0700836.

[12] J. Zhang, Y. Tian, J. Zhu, W. Zuo, L. Yin, Characterization of nitrogen transformation during microwave-induced pyrolysis of sewage sludge, J. Anal. Appl. Pyrolysis. 105 (2014) 335–341. https://doi.org/10.1016/j.jaap.2013.11.021.

[13] H. Zhan, X. Zhuang, Y. Song, X. Yin, J. Cao, Z. Shen, C. Wu, Step pyrolysis of N-rich industrial biowastes: Regulatory mechanism of NOx precursor formation via exploring decisive reaction pathways, Chem. Eng. J. 344 (2018) 320–331. https://doi.org/10.1016/j.cej.2018.03.099.

[14] A. Anca-Couce, P. Sommersacher, N. Evic, R. Mehrabian, R. Scharler, Experiments and modelling of NOx precursors release (NH3 and HCN) in fixed-bed biomass combustion conditions, Fuel. 222 (2018) 529–537. https://doi.org/10.1016/j.fuel.2018.03.003.

[15] J.P. Cao, L.Y. Li, K. Morishita, X. Bin Xiao, X.Y. Zhao, X.Y. Wei, T. Takarada, Nitrogen transformations during fast pyrolysis of sewage sludge, Fuel. 104 (2013) 1–6. https://doi.org/10.1016/j.fuel.2010.08.015.

[16] O.S. Djandja, Z.-C. Wang, F. Wang, Y.-P. Xu, P.-G. Duan, Pyrolysis of Municipal Sewage Sludge for Biofuel Production: A Review, Ind. Eng. Chem. Res. 59 (2020) 16939–16956. https://doi.org/10.1021/acs.iecr.0c01546.

[17] M. Fiore, V. Magi, A. Viggiano, Internal combustion engines powered by syngas: A review, Appl. Energy. 276 (2020) 115415. https://doi.org/10.1016/j.apenergy.2020.115415.

[18] G. Sridhar, P.J. Paul, H.S. Mukunda, Biomass derived producer gas as a reciprocating engine fuel - An experimental analysis, Biomass and Bioenergy. 21 (2001) 61–72. https://doi.org/10.1016/S0961-9534(01)00014-9.

[19] S. Szwaja, V.B. Kovacs, A. Bereczky, A. Penninger, Sewage sludge producer gas enriched with methane as a fuel to a spark ignited engine, Fuel Process. Technol. 110 (2013) 160–166. https://doi.org/10.1016/j.fuproc.2012.12.008.

[20] S. Szwaja, K. Cupial, Sewage Sludge Based Producer Gas of Rich H2 Content as a Fuel for an IC Engine, in: 18th World Hydrog. Energy Conf., Essen, Germany, 2010.

[21] A. Arunachalam, D.B. Olsen, Experimental evaluation of knock characteristics of producer gas, Biomass and Bioenergy. 37 (2012) 169–176. https://doi.org/10.1016/j.biombioe.2011.12.016.

[22] S. Bhaduri, F. Contino, H. Jeanmart, E. Breuer, The effects of biomass syngas composition, moisture, tar loading and operating conditions on the combustion of a tar-tolerant HCCI (Homogeneous Charge Compression Ignition) engine, Energy. 87 (2015) 289–302. https://doi.org/10.1016/j.energy.2015.04.076.

[23] R. Rabello de Castro, P. Brequigny, C. Mounaïm-Rousselle, A multiparameter

investigation of syngas/diesel dual-fuel engine performance and emissions with various syngas compositions, Fuel. 318 (2022) 123736. https://doi.org/10.1016/j.fuel.2022.123736.

[24] S. Tsiakmakis, D. Mertzis, A. Dimaratos, Z. Toumasatos, Z. Samaras, Experimental study of combustion in a spark ignition engine operating with producer gas from various biomass feedstocks, Fuel. 122 (2014) 126–139. https://doi.org/10.1016/j.fuel.2014.01.013.

[25] C. Lhuillier, P. Brequigny, N. Lamoureux, F. Contino, C. Mounaïm-Rousselle, Experimental investigation on laminar burning velocities of ammonia/hydrogen/air mixtures at elevated temperatures, Fuel. 263 (2020) 116653. https://doi.org/10.1016/j.fuel.2019.116653.

[26] S. Grannell, D. Assanis, D. Gillespie, S. Bohac, Exhaust Emissions From a Stoichiometric, Ammonia and Gasoline Dual Fueled Spark Ignition Engine, in: Proc. ASME Intern. Combust. Engine Divivision 2009 Spring Tech. Conf., Milwaukee, Wisconsin, USA, 2009. https://doi.org/10.1115/ICES2009-76131.

[27] C.S. Mørch, A. Bjerre, M.P. Gøttrup, S.C. Sorenson, J. Schramm, Ammonia/hydrogen mixtures in an SI-engine: Engine performance and analysis of a proposed fuel system, Fuel. 90 (2011) 854–864. https://doi.org/10.1016/j.fuel.2010.09.042.

[28] C. Lhuillier, P. Brequigny, F. Contino, C. Rousselle, Combustion Characteristics of Ammonia in a Modern Spark-Ignition Engine, SAE Tech. Pap. (2019). https://doi.org/10.4271/2019-24-0237.

[29] C. Lhuillier, P. Brequigny, F. Contino, C. Mounaïm-Rousselle, Experimental study on ammonia/hydrogen/air combustion in spark ignition engine conditions, Fuel. 269 (2020) 117448. https://doi.org/10.1016/j.fuel.2020.117448.

[30] C. Mounaïm-Rousselle, A. Mercier, P. Brequigny, C. Dumand, J. Bouriot, S. Houillé,

Performance of ammonia fuel in a spark assisted compression Ignition engine, Int. J. Engine Res. (2021) 146808742110387. https://doi.org/10.1177/14680874211038726.

[31] C. Mounaïm-Rousselle, P. Bréquigny, C. Dumand, S. Houillé, Operating Limits for Ammonia Fuel Spark-Ignition Engine, Energies 2021, Vol. 14, Page 4141. 14 (2021) 4141. https://doi.org/10.3390/en14144141.

[32] E. Koch, Ammonia as a fuel for motor buses, J. Inst. Pet. 31 (1949) 21–32.

[33] E. Monteiro, M. Bellenoue, J. Sotton, N.A. Moreira, S. Malheiro, Laminar burning velocities and Markstein numbers of syngas-air mixtures, Fuel. 89 (2010) 1985–1991. https://doi.org/10.1016/j.fuel.2009.11.008.

[34] R. Rabello de Castro, P. Brequigny, J.P. Dufitumukiza, C. Mounaïm-Rousselle, Laminar flame speed of different syngas compositions for varying thermodynamic conditions, Fuel. 301 (2021) 121025. https://doi.org/10.1016/j.fuel.2021.121025.

[35] A. Burcat, B. Ruscic, Third millenium ideal gas and condensed phase thermochemical database for combustion (with update from active thermochemical tables)., Argonne National Lab.(ANL), Argonne, IL (United States), Technion - Israel Inst. of Tech, 2005. https://doi.org/10.2172/925269.

[36] ANSYS Chemkin-Pro, (2019).

[37] E.C. Okafor, Y. Naito, S. Colson, A. Ichikawa, T. Kudo, A. Hayakawa, H. Kobayashi, Experimental and numerical study of the laminar burning velocity of CH4–NH3–air premixed flames, Combust. Flame. 187 (2018) 185–198. https://doi.org/10.1016/J.COMBUSTFLAME.2017.09.002.

[38] Gregory P. Smith, David M. Golden, Michael Frenklach, Nigel W. Moriarty, Boris Eiteneer, Mikhail Goldenberg, C. Thomas Bowman, Ronald K. Hanson, Soonho Song, William C. Gardiner, Vitali V. Lissianski, Zhiwei Qin, GRI-Mech 3.0, (n.d.). http://combustion.berkeley.edu/gri-mech/version30 (accessed April 25, 2022).

[39] Z. Tian, Y. Li, L. Zhang, P. Glarborg, F. Qi, An experimental and kinetic modeling study of premixed NH3/CH4/O2/Ar flames at low pressure, Combust. Flame. 156 (2009) 1413–1426. https://doi.org/10.1016/j.combustflame.2009.03.005.

[40] J. Zheng, J. Wang, Z. Zhao, D. Wang, Z. Huang, Effect of equivalence ratio on combustion and emissions of a dual-fuel natural gas engine ignited with diesel, Appl. Therm. Eng. 146 (2019) 738–751. https://doi.org/10.1016/j.applthermaleng.2018.10.045.

[41] V.G. Bui, T. Minh, T. Bui, V.N. Tran, Z. Huang, A.T. Hoang, W. Tarelko, V.H. Bui, X.M. Pham, P. Quy, P. Nguyen, Flexible syngas-biogas-hydrogen fueling spark-ignition engine behaviors with optimized fuel compositions and control parameters, (2022). https://doi.org/10.1016/j.ijhydene.2022.09.133.

[42] P. Kumar Sharma, A. Kumar Sharma, S. Shenbagaraj, S. Mondal, An investigation on emissions analysis of spark plug engine fueled by producer gas generated by L. camera, (2021). https://doi.org/10.1016/j.matpr.2021.02.615.

[43] A. Shah, R. Srinivasan, S. D. Filip To, E.P. Columbus, Performance and emissions of a spark-ignited engine driven generator on biomass based syngas, Bioresour. Technol. 101 (2010) 4656–4661. https://doi.org/10.1016/J.BIORTECH.2010.01.049.

[44] K.P. Shrestha, C. Lhuillier, A.A. Barbosa, P. Brequigny, F. Contino, C. Mounaïm-Rousselle, L. Seidel, F. Mauss, An experimental and modeling study of ammonia with enriched oxygen content and ammonia/hydrogen laminar flame speed at elevated pressure and temperature, Proc. Combust. Inst. 38 (2021) 2163–2174. https://doi.org/10.1016/j.proci.2020.06.197.

[45] G.B. Ariemma, G. Sorrentino, R. Ragucci, M. De Joannon, P. Sabia, Ammonia/Methane combustion: Stability and NO x emissions, Combust. Flame. 241 (2022) 112071. https://doi.org/10.1016/j.combustflame.2022.112071.